RSC Advances

PAPER

View Article Online
View Journal | View Issue

Cite this: *RSC Adv.*, 2020, **10**, 8140

Synthesis of dendritic fibrous nanosilica over a cubic core (cSiO$_2$@DFNS) with catalytically efficient silver nanoparticles for reduction of nitroarenes and degradation of organic dyes

Javaid Shabir, Swati Rani, Manisha Sharma, Charu Garkoti, Surabhi and Subho Mozumdar *

In this study, dendritic fibrous core–shell silica particles having cubic morphology with uniform and vertical nanochannels have been successfully synthesised. The synthesized dendritic fibrous nanosilica over a cubic core (cSiO$_2$@DFNS) have been characterized by using various techniques, such as powder X-ray diffraction, TEM, FE-SEM, TGA EDS, FT-IR and N_2 adsorption–desorption experiments. The prepared DFNS particles demonstrated a very high surface area and pore diameter. Amine groups were functionalized on the fibres of cSiO$_2$@DFNS and after that silver nanoparticles could be successfully immobilized on amine functionalized cubic silica particles. Due to the presence of a high surface area and a uniform pore diameter, the silver nanoparticle loaded cSiO$_2$@DFNS could be successfully employed as an efficient and recoverable catalyst for reduction of toxic aromatic nitro compounds and degradation of organic dyes. Higher catalytic activity of the prepared material could be attributed to its fibrous morphology which could facilitate proper interactions of the reactants molecules with the silver nanoparticles.

Received 14th January 2020
Accepted 15th February 2020

DOI: 10.1039/d0ra00402b

rsc.li/rsc-advances

1. Introduction

In the recent past, there have been significant advances in the fabrication of silica based porous solid materials with different morphologies and ordered structures.[1–6] It has been shown that ordered mesoporous materials with nanoscopic space can have a wide range of applications in numerous research areas including biomedicine, chemical separation, energy storage, environmental remediation, heterogeneous catalysis and many multi-disciplinary research fields.[7–11] In the recent era, a large numbers of reports have been published where tremendous efforts have been made in synthesizing mesoporous silica nanospheres, primarily as a support material, for heterogenizing the homogeneous catalysts.[12] Mostly surfactant and amphiphilic block copolymers have been used as structural directing templates so as to control the morphology and pore size of silica based porous materials.[13]

In a report by Polshettiwar *et al.*, the synthesis of very novel and interesting dendritic fibrous silica nanospheres (famously called KCC-1 or DFNS) using a microwave assisted hydrothermal technique has been described.[1] Due to the fibrous morphology of DFNS, there is nanoscopic space between the adjacent fibres and this results in high surface area and a larger pore volume. The fibres of DFNS could be easily functionalized with active functional moieties.[11] Due to the high surface area and available nanoscopic space for functionalization of active moieties, DFNS have been extensively used as an inorganic solid support material for heterogenizing the homogeneous catalysts. In the past, different acidic and basic catalytically active moieties have been immobilized on DFNS so as to obtain an efficient and recoverable catalyst for various organic transformations.[14–18] A number of different kinds of metal nanoparticles have also been immobilised on amine supported DFNS and further they have been employed as efficient catalysts for numerous organic transformations including C–C coupling reactions.[19–23] Kejie *et al.* have reported the synthesis of fibrous core–shell structure (Fe_3O_4/SiO_2/DFNS)[24] and these have been extensively used by the scientific community as a solid support material for developing heterogeneous catalysts.[9,20] Due to the presence of Fe_3O_4 as a magnetic core in Fe_3O_4/SiO_2/DFNS, it has the additional advantage of being magnetically recyclable when employed as heterogeneous catalysts. However, in both DFNS and in Fe_3O_4/SiO_2/DFNS, the distance between two adjacent fibres is non-uniform because of their spherical morphologies. Since the pore is V-shaped, the pore size is maximum at the surface and it gradually decreases starting from the outer surface to the interior of the nanosphere. It is, therefore, speculated that due to the non-uniform pore size, the guest molecules may not be able to have full access to the active moieties grafted on the fibres of the silica nanospheres especially at interior, when used for different applications including heterogeneous catalysis.

Department of Chemistry, University of Delhi, Delhi–110007, India. E-mail: subhoscom@yahoo.co.in; Tel: +91 9810728438

The control on the orientation of mesopores in silica nanospheres is a widely explored topic in the scientific community. Ordered mesoporous silica materials having large and uniformly sized nanochannels starting from the outer surface to the inner core have been used for applications involving the host–guest interaction with active functional groups or metal nanoparticles.[25–27] One can imagine that nanochannels perpendicular to the template material having a uniform size can avoid the problem of pore blocking during interaction with guest species. Such types of materials possessing uniform nanoscopic space can provide very effective and unique confinement for conducting host–guest chemistry at a nanoscale.

Dendritic fibrous nanosilica over cubic core ($cSiO_2$@DFNS) is being reported here in this article. The prepared $cSiO_2$@DFNS have almost uniform distance between the two adjacent fibres and thus possess uniform pore size (nanoscopic space starting from surface to the interior). Initially, silica nanocubes ($cSiO_2$) have been synthesized by using the already reported method[28] and then, these silica nanocubes have been used as a core material to synthesize the fibrous shell of silica over it and the final product was named as dendritic fibrous nanosilica over cubic core ($cSiO_2$@DFNS). While doing so, cetylpyridinium bromide (CPB) and TEOS have been used as structural directing template and as the silica source, respectively. The obtained fibrous silica nanocubes $cSiO_2$@DFNS possess a very high surface area, larger pore volume and most importantly nanochannels or pores having uniform size. These morphological properties are very important for the number of applications and especially when these uniform nanospaces are being explored to confine the metal nanoparticles for catalytic applications. In the continuation of our efforts to design and synthesize the nanostructured material for catalytic applications.[29–34] Confinement of the silver nanoparticles in the nanochannels of this newly designed dendritic fibrous nanosilica over cubic core ($cSiO_2$@DFNS) is being reported in this article. The obtained core–shell fibrous silica particles with supported Ag nanoparticles ($cSiO_2$@DFNS@Ag) have been employed as an efficient catalyst in the reduction of nitroarenes and degradation of organic dyes using $NaBH_4$ as reducing agent. The catalyst showed excellent catalytic activity and it could be recovered and reused for multiple catalytic cycles without any appreciable loss in the catalytic activity. This protocol is aimed at further investigation of silica based mesoporous material having uniform pore size for immobilising active functional groups for various other applications.

2. Experimental

2.1. Materials

Tetraethyl orthosilicate (TEOS), and cetyltrimethylammonium bromide (CTAB) were purchased from Sigma-Aldrich. Silver nitrate ($AgNO_3$), 3-aminopropyltriethoxysilane (APTES) and cetylpyridinium bromide (CPB) were purchased from Alfa Aesar. All the other chemicals that were used are purchased from Thomas Baker, Spectrochem, and Merck. All the reagents were used without any further purification.

2.2. Synthesis of ordered cubic silica ($cSiO_2$) particles

The synthesis of silica nanocubes ($cSiO_2$) is based on Stöber method.[28] In the typical synthesis procedure, 160 mL of deionized water was taken in a 500 mL round bottom flask and 1.0 g of CTAB was then dissolved in it under continuous stirring. Then, 7.0 mL of concentrated ammonia solution (28 wt%) was added into water–CTAB mixture, forming a clear solution. After that, 25 mL of TEOS (20 V/V% in *n*-hexane) was drop wise added into the solution under continuous stirring. After 12 h of relaxed stirring of the reaction mixture at 35 °C, the cubic silica particles were collected by centrifuging the reaction mixture at 4000 rpm. The product was washed with deionized water and ethanol for several times and dried in a vacuum oven for 6 hours. The solid sample was calcined in air at 550 °C to remove the CTAB template.

2.3. Synthesis of dendritic fibrous nanosilica over cubic core ($cSiO_2$@DFNS)

Dendritic fibrous shell was synthesised on the silica cubes using the reported protocol.[24] Typically, 250 mg silica cubes ($cSiO_2$) were dispersed into 30 mL of deionized water containing urea (300 mg) to form solution A under ultrasonication. Meanwhile, 500 mg cetylpyridinium bromide (CPB) was added to 30 mL of cyclohexane and after that 750 μL of *n*-pentanol was added to form solution B also under ultrasonication. Solution A was added to solution B under continuous stirring at room temperature. Then, 1.2 mL TEOS was added dropwise under relaxed stirring. The resulting reaction mixture was continuously stirred at room temperature for 1 h then heated to 110 °C environment for 6 h. After the completion of the reaction, the product ($cSiO_2$@DFNS) was collected by centrifugation of the reaction mixture at 4000 rpm, the product was thoroughly washed with deionized water and methanol and then dried in vacuum oven for 6 h. CPB template was removed by calcining the as-synthesized material at 550 °C for six hours in the air.

2.4. Preparation of amine functionalized $cSiO_2$@DFNS

The amine-functionalized $cSiO_2$@DFNS were synthesized *via* a postgrafting protocol. In a typical process, 250 mg of extracted DFNS were mixed with 20 mL of anhydrous toluene in a 100 mL round-bottomed flask and sonicated for 5 minutes and then vigorously stirred for 30 min. After that, 0.250 mL of 3-aminopropyltriethoxysilane (APTES) was added to the toluene dispersion of $cSiO_2$@DFNS. The reaction was refluxed at 110 °C in a nitrogen atmosphere for 24 h. After the completion of the reaction, amine functionalized $cSiO_2$@DFNS were collected by centrifugation of the reaction mixture. The amine functionalized product was washed with ethanol several times and dried overnight in a vacuum oven.

2.5. Immobilization of silver nanoparticles over $cSiO_2$@DFNS

In a typical procedure, amine functionalized $cSiO_2$@DFNS (150 mg) were dispersed into 20 mL deionized water *via* ultrasonication for 20 min. Afterwards, $AgNO_3$ (30 mg) was added and the reaction

mixture was stirred for 1.5 h at 30 °C. Subsequently, an excess amount of freshly prepared 0.1 M $NaBH_4$ solution was added drop wise. The resulting solution was stirred for 2 h at the same temperature. The product $cSiO_2$@DFNS@Ag were separated by centrifugation and repeatedly washed with DI water followed by ethanol and then finally dried in vacuum oven at 60 °C.

2.6. General procedure for the catalytic reduction of nitroarenes

Typically, 0.2 mM aqueous solution of aromatic nitro compound (2.2 mL) was taken in a standard cuvette having 3 mL volume and 1 cm path length. Then after, 0.3 mL of 0.2 M aqueous $NaBH_4$ solution was added into the same cuvette, followed by the addition of 200 μL of aqueous dispersion of $cSiO_2$@DFNS@Ag (0.2 mg, 1 mg mL^{-1}) as nanocatalyst. The UV-vis absorption spectra of the reaction mixture were recorded immediately at constant time intervals at room temperature.

2.7. General procedure for the catalytic degradation of organic dyes

In the typical procedure, 2 mL of 0.02 mM aqueous solution of organic dye was placed in a quartz cuvette of 3 mL volume and 1 cm length. Subsequently, 0.4 mL of 0.1 M aqueous $NaBH_4$ solution was added into the same cuvette followed by the addition of 200 μL of aqueous dispersion of $cSiO_2$@DFNS@Ag (0.2 mg, 1 mg mL^{-1}) as nanocatalyst. The UV-vis absorption spectra of the reaction mixture at room temperature were repeatedly recorded at constant time intervals.

3. Characterization techniques

Scanning electron microscopy (SEM) and transmission electron microscopy (TEM) analysis were performed on the samples regarding the information about their morphology and size. Fourier transform infrared (FT-IR) spectra were recorded in the range of 4000–400 cm^{-1} using KBr pellet method through a PerkinElmer Spectrum RXI-Mid IR spectrometer. For elemental mapping of the samples, energy-dispersive X-ray spectroscopic (EDS) (equipped with the SEM instrument) was performed on the samples. Powder X-ray diffraction (XRD) of the samples were recorded by using a Bruker, D8 Discover diffractometer with Cu, 3 kW at a scanning rate of 4° min^{-1} in the 2θ range of 5–80°. Nitrogen adsorption–desorption experiment was carried using Quantachrome Instruments, Model ASI-CI-11 analyzer. The Brunauer–Emmett–Teller (BET) method was used to calculate the specific surface areas and the pore diameter of the prepared samples.

4. Results and discussion

The dendritic fibrous cubic silica with efficient silver nanoparticles ($cSiO_2$@DFNS@Ag) were synthesized in a step-wise synthetic procedure as depicted in Scheme 1. Initially, cubic silica particles ($cSiO_2$) were synthesized by a nonpolar solvent-assisted Stöber method by using cetyltrimethylammonium bromide (CTAB) as a structural directing template and tetraethyl orthosilicate (TEOS) as a silica source.[28] The morphology of the prepared cubic silica particles ($cSiO_2$) was analyzed by using transmission electron microscopy (TEM) and scanning electron microscopy (SEM). Based on the TEM and SEM analysis, it was clear that the prepared silica particles had a highly ordered cubic morphology and the particles were highly monodispersed without any agglomeration. In the next step, the $cSiO_2$ particles were utilized as a core material and a dendritic fibrous nanosilica shell (DFNS) was developed on it. In this procedure, the surfactant cetylpyridinium bromide (CPB) was used as a structural directing template and TEOS as a silica precursor in a base catalysed reaction using *n*-hexane–water bi-phase system. In the third step of synthesis procedure, the prepared $cSiO_2$@DFNS silica particles were functionalized with amine group using 3-aminopropyltriethoxysilane (APTES) in anhydrous toluene as a solvent. Finally, Ag^+ ions were loaded on the prepared $cSiO_2$@DFNS using a ligand assisted approach, where NH_2 groups were acting as ligand so as to attract Ag^+. In the last step of the synthetic procedure, $NaBH_4$ was used to reduce the Ag^+ ions to Ag nanoparticles. The prepared Ag nanoparticles were uniformly dispersed on the fibres of $cSiO_2$@DFNS and they could be stabilized by the amine groups.

4.1. Characterisation

Morphology, shape, size and structural features of the prepared cubic silica particles ($cSiO_2$), dendritic fibrous nanosilica over cubic core ($cSiO_2$@DFNS) and silver nanoparticle immobilized over $cSiO_2$@DFNS were analysed by TEM and FE-SEM analysis of the samples. Based on the images obtained through TEM (Fig. 1a and b), it was quite clear that the core material *i.e.* cubic silica particles ($cSiO_2$) were very well dispersed without any agglomeration and had well defined cubic morphology with ordered structure that agreed well with the observation made through FE-SEM analysis of the samples (Fig. 1c and d). Both SEM and TEM analysis confirmed the particle size of cubic silica particles to be around 200 nm.

Subsequent to fabricating of dendritic fibrous shell around the cubic core, the obtained fibrous silica particles ($cSiO_2$@DFNS) were analysed for their structural features using FE-SEM and TEM (Fig. 2). The $cSiO_2$@DFNS particles were highly monodispersed without any aggregation and had well-defined and ordered structure with a cubic morphology and a slightly round in shape near the corners of the cube. The TEM (Fig. 2a and b) and SEM (Fig. 2b and c) analysis were in close agreement about the structural features of the prepared fibrous cubic material. It may be noted that some spherical dendritic fibrous silica particles (DFSP) could also be observed in the TEM analysis as a by-product and that could be due to competitive homogeneous nucleation and growth together with the heterogeneous ones. The size of the core–shell dendritic fibrous silica particles ($cSiO_2$@DFNS) was found to be about 300 nm from both SEM and TEM analysis. Finally, following the grafting of the amine group on the fibres of the $cSiO_2$@DFNS, silver nanoparticles could be immobilised on $cSiO_2$@DFNS (because of the presence of nanoscopic space between the fibres). The prepared material *i.e.* $cSiO_2$@DFNS@Ag was visualized through TEM analysis (Fig. 3) and it was found that silver

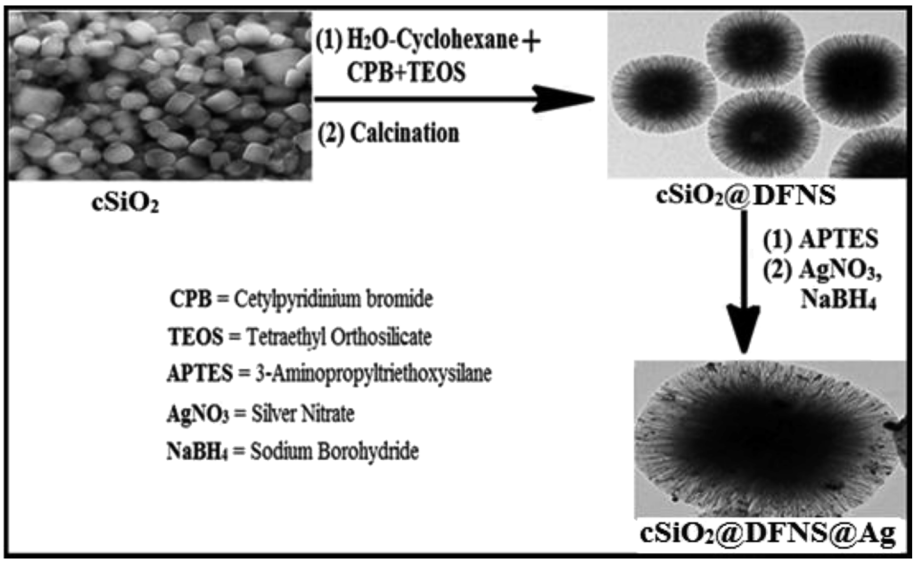

Scheme 1 Schematic representation of step wise synthesis of $cSiO_2$@DFNS@Ag nanocatalyst.

nanoparticles were highly dispersed over $cSiO_2$@DFNS@Ag, with the size of silver nanoparticles being about 10 nm.

In the FT-IR spectrum (Fig. 4) of $cSiO_2$@DFNS, the characteristic peaks at 803.1 cm^{-1}, 967 cm^{-1} and 1084 cm^{-1} could be due to the symmetric stretching vibrations and asymmetric stretching vibrations of O–Si and Si–O–Si bonds. The broader peak observed at 3434.30 cm^{-1} in the spectrum of $cSiO_2$@DFNS could be assigned to a large number of Si–OH groups. Following grafting of the amine groups on the surface of $cSiO_2$@DFNS, an emergence of a new peak at 2925 cm^{-1} could be seen and this confirmed the incorporation of 3-APTES over the surface of $cSiO_2$@DFNS. This new peak could be assigned to the vibration of the alkyl chain present in the structure of the 3-APTES molecule.

Thermogravimetric (TGA) analysis was performed to further confirm the grafting of 3-APTES on the surface of $cSiO_2$@DFNS. In the TGA curve of $cSiO_2$@DFNS, a very slight weight loss was observed below 250 °C (Fig. 5).

This weight loss could be due to the loss of physisorbed water on the silica surface. In the case of $cSiO_2$@DFNS-NH_2, weight loss was observed at a higher temperature between 180 °C to 600 °C and this could be mainly due to the decomposition of 3-APTES groups grafted on the fibres of $cSiO_2$@DFNS. In order to further confirm the grafting of 3-APTES on $cSiO_2$@DFNS, CHN analysis of samples was carried out and we observed that weight percentage of nitrogen in $cSiO_2$@DFNS@NH_2 {N (wt%)} was found to 2.94%.

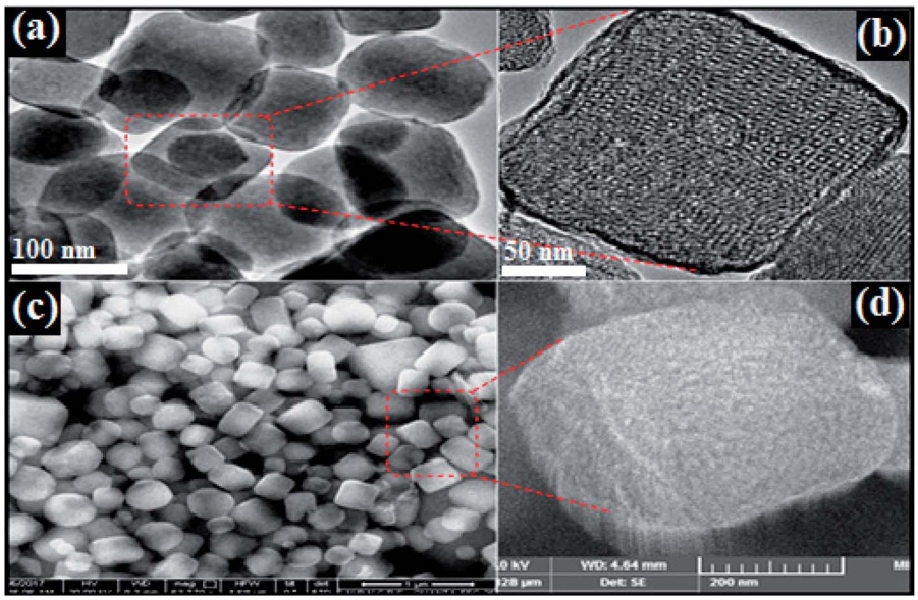

Fig. 1 TEM image of $cSiO_2$ (a and b), FE-SEM image of $cSiO_2$ (c and d).

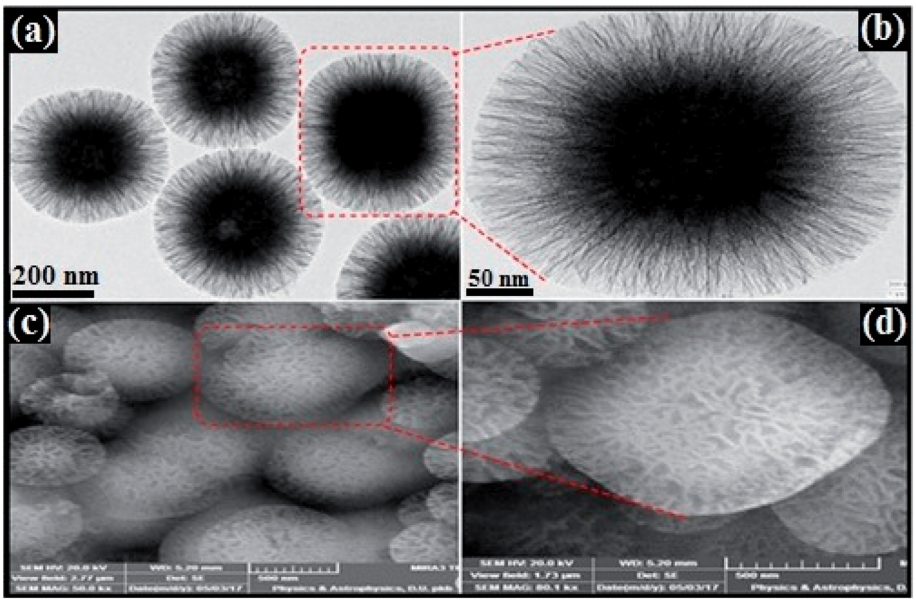

Fig. 2 TEM images of $cSiO_2$@DFNS (a and b), FE-SEM images of $cSiO_2$@DFNS (c and d).

The powder XRD patterns of the prepared $cSiO_2$@DFNS showed a broad characteristic peak of amorphous silica in the range of 2θ from 15° to 30° (Fig. 6). However, following immobilization of the silver nanoparticles on the fibres of $cSiO_2$@DFNS, four new peaks could be observed in the XRD pattern of $cSiO_2$@DFNS@Ag at 2θ diffraction angles of 38.15°, 44.33°, 64.43° and 77.41° corresponding to (111), (200), (220) and (311) planes respectively. These planes correspond to the FCC structure of silver nanoparticles (JCPDS no. 00-004-0783).

The elemental composition of the prepared materials $cSiO_2$@DFNS and $cSiO_2$@DFNS@Ag was determined through EDS analysis (equipped with the SEM instrument). In case of $cSiO_2$@DFNS there was the characteristic peak of Si (silicon) and O (oxygen) only and after the immobilization of uniformly dispersed Ag nanoparticle in the nanoscopic channels of $cSiO_2$@DFNS, the characteristic prominent peak of Ag appears in the EDS spectrum of $cSiO_2$@DFNS@Ag (Fig. 7). This presence of Ag peak in the EDS spectrum of the $cSiO_2$@DFNS@Ag

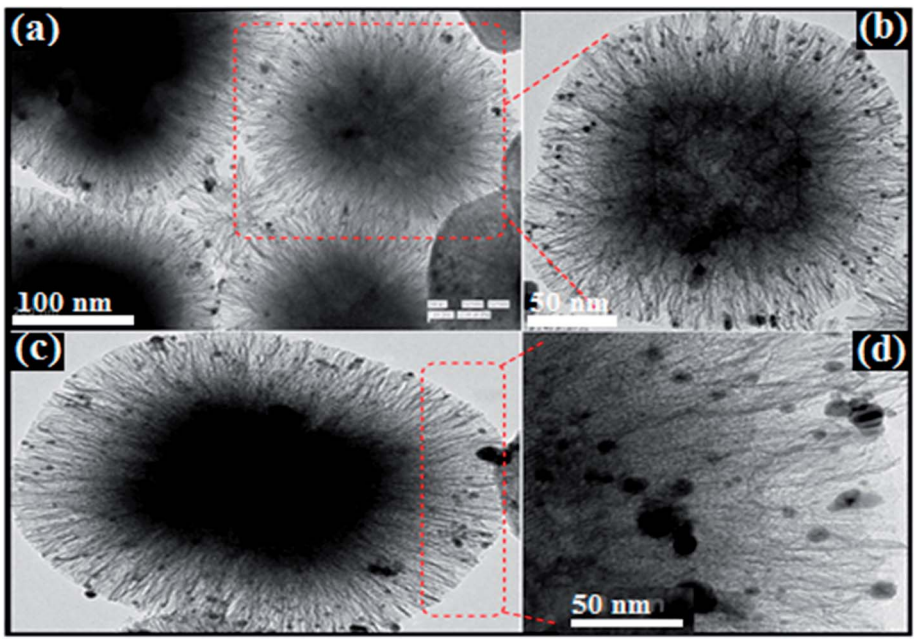

Fig. 3 TEM images of $cSiO_2$@DFNS@Ag at different magnifications.

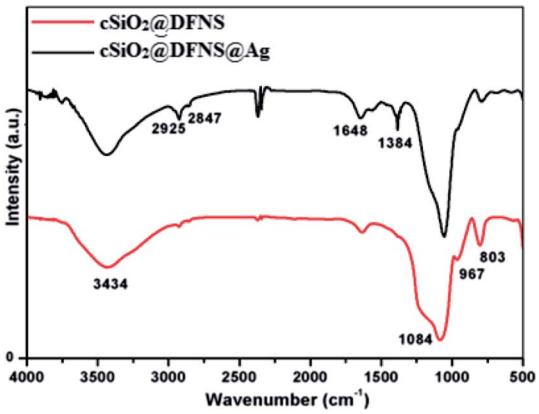

Fig. 4 FT-IR spectra of $cSiO_2$@DFNS and $cSiO_2$@DFNS-NH_2.

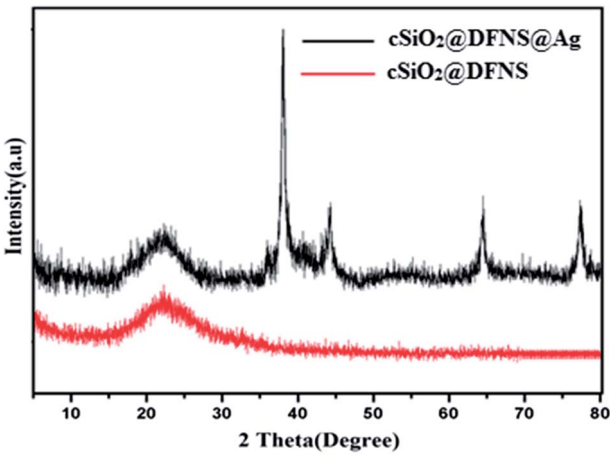

Fig. 6 Powder X-ray diffraction pattern of $cSiO_2$@DFNS@Ag (black) and $cSiO_2$@DFNS (red).

confirmed that silver nanoparticles were successfully and uniformly immobilized. The accurate weight percentage of Ag in the $cSiO_2$@DFNS@Ag was determined through ICP analysis and was found to be 3.57 wt%.

N_2 adsorption–desorption isotherms of $cSiO_2$@DFNS exhibited typical type-IV curves (Fig. 8). Prior to BET analysis, the samples were degassed for 12 h at 120 °C under vacuum. The BET surface area of $cSiO_2$@DFNS was found to be 702.76 $m^2\ g^{-1}$ and the total pore volume was 1.9 $cm^3\ g^{-1}$. The pore diameter was found to be approximately 10 nm. The higher surface area and larger pore diameter confirmed that $cSiO_2$@DFNS is a highly porous material with almost uniform nanoscopic space between the fibres. Such type of material, when employed as a solid support material in designing the heterogeneous catalytic system, can have the advantage of higher accessibility of catalytic active group by the reacting molecules, which can result in an increased rate of reaction and higher yield of the product. Hence, these properties could make the $cSiO_2$@DFNS@Ag as a potential candidate for designing an effective heterogeneous nanocatalyst.

4.2. Catalytic activity

In order to examine the catalytic efficiency of the synthesized $cSiO_2$@DFNS@Ag, it was employed as a heterogeneous nanocatalyst for the reduction of hazardous nitroarenes to their corresponding aromatic amine in the presence of reducing agents like $NaBH_4$. In addition, catalytic degradation of various harmful organic dyes has also been studied by employing the prepared material *i.e.* $cSiO_2$@DFNS@Ag as a recyclable nanocatalyst.

4.2.1. Catalytic reduction of nitroarenes. To check the catalytic activity of the prepared material *i.e.* $cSiO_2$@DFNS@Ag, reduction of 4-nitrophenol (4-NP) to 4-aminophenol (4-AP) using $NaBH_4$ as reducing agent was chosen as the first model reaction. The progression of this reaction could be easily monitored through UV-visible absorption spectroscopy (Fig. 9). The light yellow colour of an aqueous solution of 4-NP showed absorption peak at 317 nm and after the addition of $NaBH_4$, the

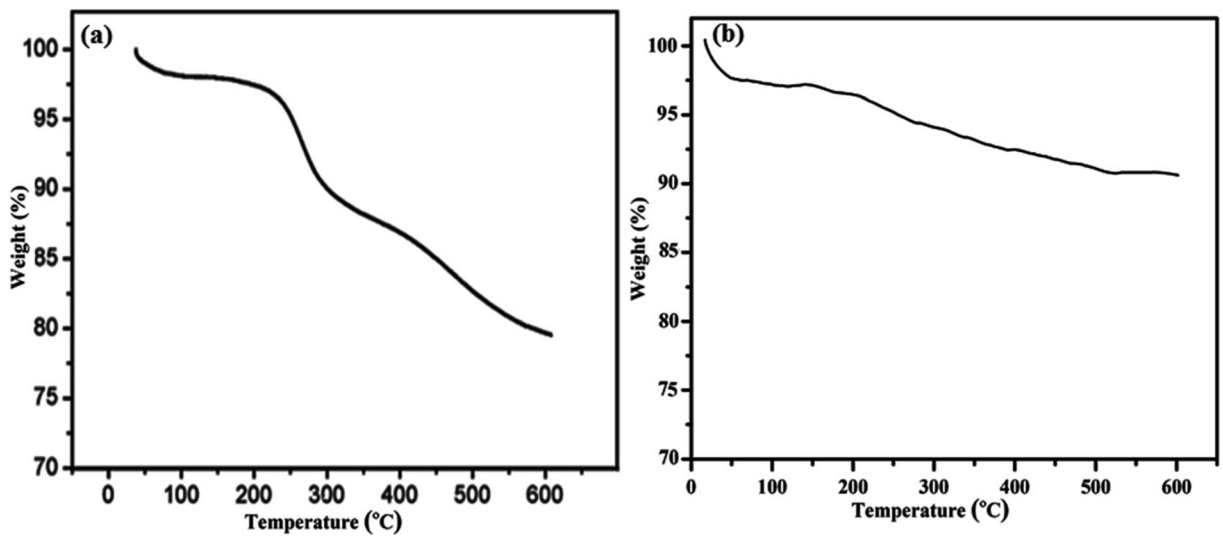

Fig. 5 Thermogravimetric analysis of (a) $cSiO_2$@DFNS@NH_2. (b) $cSiO_2$@DFNS.

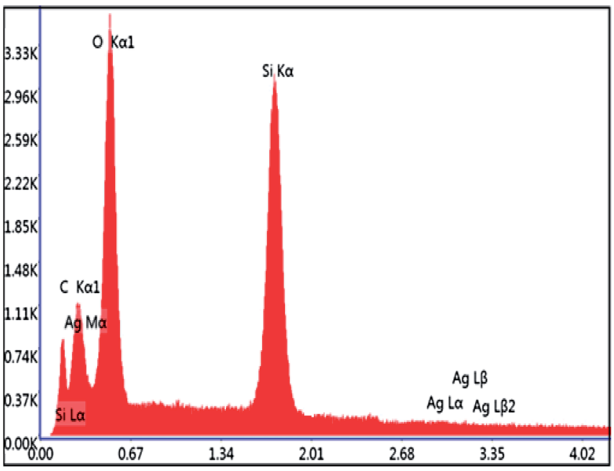

Fig. 7 EDS spectrum of $cSiO_2$@DFNS@Ag.

colour of 4-NP changed to deep yellow from light yellow. This colour could be due to the change in the alkalinity of the solution. The increase in alkalinity due to addition of $NaBH_4$ could result in the formation of 4-nitrophenolate ion. The absorption peak of the 4-nitrophenolate ion changed accordingly and was observed at 400 nm, which remained unchanged even up to 45 minutes. However, after that addition of a 0.2 mg of the prepared material (*i.e.* $cSiO_2$@DFNS@Ag) as nanocatalyst into the reaction mixture, the intensity of the absorption peak of 4-nitrophenolate ion (at 400 nm) decreased rapidly over a period of time and a new peak was observed to rise at 300 nm. This new peak is due to the formation of 4-aminophenol (4-AP). It was further observed that the peak at 400 nm completely disappeared after 140 seconds and this indicated the complete reduction of 4-NP. Correspondingly, the colour of the reaction mixture was also seen to change from deep yellow to colourless (as observed visually in the quartz cuvette).

Apart from the reduction of 4-NP, the prepared catalyst was also checked for its activity in the reduction of 4-nitroaniline (4-NA) and 2-nitroaniline (2-NA). UV-vis absorption spectra for the catalytic reduction of 4-NA and 2-NA (in the presence of $NaBH_4$ as reducing agent) and 0.2 mg of the prepared catalyst are shown in Fig. 9b and c, respectively. In case of 4-NA, the intensity of absorption peak at 380 nm gradually decreased after the addition of $cSiO_2$@DFNS@Ag as nanocatalyst and completely disappeared after 140 seconds. Two new absorption peaks appeared in the UV-vis spectra at 240 nm and 300 nm and these peaks could be attributed to the formation of the amine product. Similarly, after the addition of nanocatalyst ($cSiO_2$@DFNS@Ag) to the mixture of 2-NA and $NaBH_4$, the intensity of absorption peak at 420 nm completely vanished after 160 seconds, indicating the complete reduction of 2-NA with the formation of the corresponding amine product (Fig. 9c). In these experiments, the concentration of $NaBH_4$ (0.2 M) is much higher in comparison to that of nitroarenes (0.2 mM) and therefore the concentration of $NaBH_4$ could be considered as a constant during the course of the reaction. The reactions are thus considered as pseudo first order and therefore first order kinetics has been applied to calculate the catalytic efficiency of the $cSiO_2$@DFNS@Ag for the reduction of nitroarenes. For the kinetic studies, the progress of the reaction at time t can be monitored by calculating (C_t/C_0). Here, (C_t/C_0) can be measured from the relative absorbance intensity (A_t/A_0) of 4-NP, 2-NA and 4-NA (A_t is the absorbance value at $t = t$ and A_0 is the absorbance at $t = 0$). The rate constant k of the reduction reactions could be calculated from the linear plots of $\ln(C_t/C_0)$ *vs.* reaction time (Fig. 9d). Here, (C_t/C_0) is the ratio of concentration at a certain time t to that at the initial time ($t = 0$). The values of rate constant k for 4-NP, 2-NA and 4-NA are tabulated in (Table 1).

In order to compare the catalytic activity of the prepared catalyst *i.e.* $cSiO_2$@DFNS@Ag with some of the reported catalyst in the literature, the rate constants k were normalized and represented in terms of activity parameter "K". Activity parameter is equal to the ratio of rate constant with the amount of catalyst taken for the catalysis, mathematically, $K = k/m$ (k is rate constant and m is the amount of catalyst). Herein, we have compared the activity parameters of the $cSiO_2$@DFNS@Ag for the reduction of 4-NP with some of the reported nanocatalysts and the results are incorporated in Table 2.[35–38] From the results tabulated in Table 2, it was observed that the prepared nanocatalyst is more efficient as compared to the reported protocols.

4.2.2. Catalytic degradation of organic dyes. There are number of organic dyes, such as rhodamine B, methyl orange, methyl red and methylene blue that have applications in industries and are also used for biological tagging. These organic dyes have very harmful effect on our environment and especially when they are released into the aquatic systems. The degradation of these harmful organic dyes is necessary before their discharge into the water bodies. Here, we have utilized the prepared catalyst ($cSiO_2$@DFNS@Ag) for the degradation of some of the organic dyes such as rhodamine B (RhB), methyl orange (MO) and methylene blue (MB).

The degradation of rhodamine B (RhB) by $NaBH_4$ was studied in the presence of $cSiO_2$@DFNS@Ag as nanocatalyst. The UV-vis absorption spectra of the degradation of RhB are shown in Fig. 10a.

It is observed that 2 mL of 0.02 mM RhB have a characteristics peak at 554 nm and after the addition of 0.2 mg of prepared

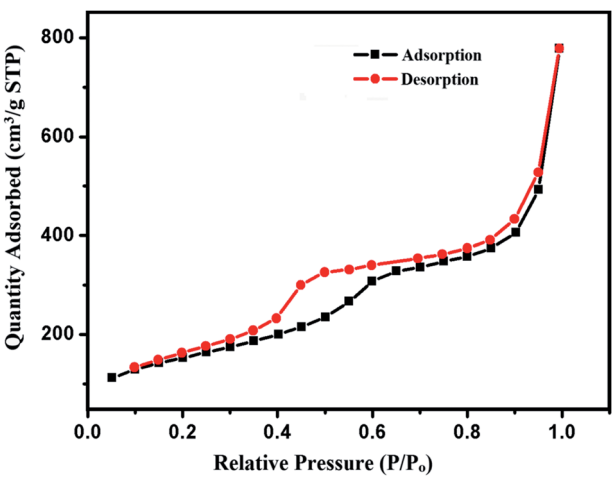

Fig. 8 N_2 adsorption–desorption isotherm of $cSiO_2$@DFNS.

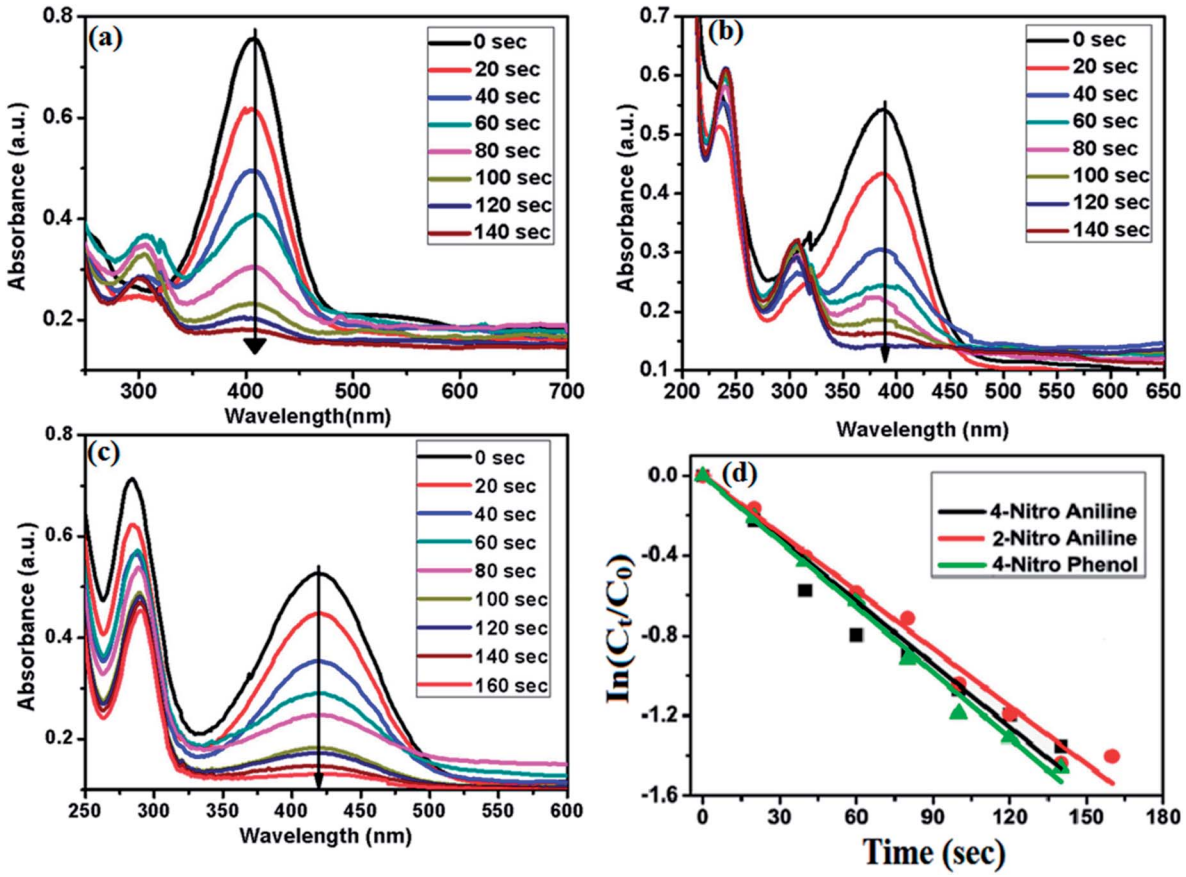

Fig. 9 UV-vis absorption spectra for the reduction of 0.2 mM (a) 4-NP; (b) 4-NA and (c) 2-NA in the presence of 0.2 mg $cSiO_2$@DFNS@Ag as nanocatalyst and (d) plot of $\ln(C_t/C_0)$ *vs.* time representing first order kinetics for the reduction of nitroarenes.

catalyst *i.e.* $cSiO_2$@DFNS@Ag and $NaBH_4$ (0.1 M), the characteristic peaks at 554 nm started decreasing gradually and disappears completely after 220 s. The degradation did not occur in the absence of catalyst and the characteristic peaks of RhB at 554 nm remained there even after 30 minutes, which confirms that the degradation is only possible in the presence of the catalyst. The catalyst provides surface area for the adsorption of reacting species (organic dye and $NaBH_4$) which facilitates the faster electrons transfer between them resulting in the rapid degradation of the organic dyes. The degradation of methyl orange (MO) and methylene blue (MB) were performed similarly as discussed in the case of RhB *i.e.* by using 0.2 mg of $cSiO_2$@DFNS@Ag as nanocatalyst. The Fig. 10b shows the degradation of MO and it was observed that the characteristic absorption peak of MO is cantered at 464 nm and after the addition of $cSiO_2$@DFNS@Ag as nanocatalyst, this peak completely disappeared after 200 s. Similarly the prepared catalyst was also utilized for the degradation of methylene blue having characteristic peak at 664 nm in UV-vis absorption spectra (Fig. 10c). After the addition of 0.2 mg of $cSiO_2$@DFNS@Ag in the mixture consisting of MB and $NaBH_4$ (0.1 M), the absorption peak cantered at 664 nm completely vanished after 160 s. The rate constant '*k*' for the degradation of organic dyes were calculated similarly as calculated for nitroarenes *i.e.* by considering the degradation reactions to be pseudo first order (because the concentration of $NaBH_4$ utilized here is also much higher than that of organic dyes and remained unchanged during the course of the reaction). The rate constant '*k*' was calculated by applying first-order kinetics. The rate

Table 1 The correlation coefficient of $\ln(C_t/C_0)$ *vs.* time plot, reduction time, rate constant and activity parameter for the reduction of nitroarenes using $cSiO_2$@DFNS@Ag as heterogeneous nanocatalyst

Sample	R^2	Reduction time (s)	k ($\times 10^{-3}$ s^{-1})	Activity parameter ($K = s^{-1} g^{-1}$)
4-Nitro phenol	0.997	140	10.93	54.65
2-Nitro aniline	0.9942	160	9.62	48.1
4-Nitro aniline	0.987	140	10.48	52.4

Table 2 Comparison of the catalytic activity of $cSiO_2$@DFNS@Ag with some previously reported catalysts for the reduction of 4-NP

Entry	Catalyst	Catalyst amount (mg)	k ($\times 10^{-3}$ s^{-1})	Activity parameter ($K = s^{-1}$ g^{-1})	Reference
1	KCC-1@Ag	0.2	10	50	35
2	Ag@SBA-15	0.9	12.7	14.1	36
3	Fe_3O_4@SiO_2–Ag	1.0	7.67	7.67	37
4	Ag/carbon sphere	1.0	1.69	1.69	38
5	$cSiO_2$@DFNS@Ag	0.2	10.93	54.65	This work

constant and activity parameters for the degradation of RhB, MO and MB has been obtained from the linear plot of $\ln(C_t/C_0)$ *vs.* degradation time (Fig. 10d) and the same has been presented in Table 3.

The outstanding catalytic efficiency shown by the $cSiO_2$@DFNS@Ag could be due to the fibrous morphology of the $cSiO_2$@DFNS@Ag, having larger and uniform nanoscopic space between the adjacent fibres. Due to the larger and almost uniform pore size, the probability of effective interaction between the reacting species and the catalytic active site could be very high and this could result in the high yield of the product.

4.3. Recyclability test

Finally, the recyclability of the $cSiO_2$@DFNS@Ag nanocatalyst was tested and it was found that the catalyst could be used for five consecutive catalytic cycles for the reduction of 4-NP as well as degradation of RhB without any noticeable loss in its activity (Fig. 11a and b). The catalyst could be easily recovered through centrifugation followed by washing thoroughly with water and ethanol and finally drying in the vacuum oven for further use. Study regarding the leaching of the active catalytic sites is also very important in heterogeneous catalysis. In order to investigate the leaching of the catalytic sites (*i.e.* silver nanoparticles) into the reaction mixture, the filtration test was carried out.

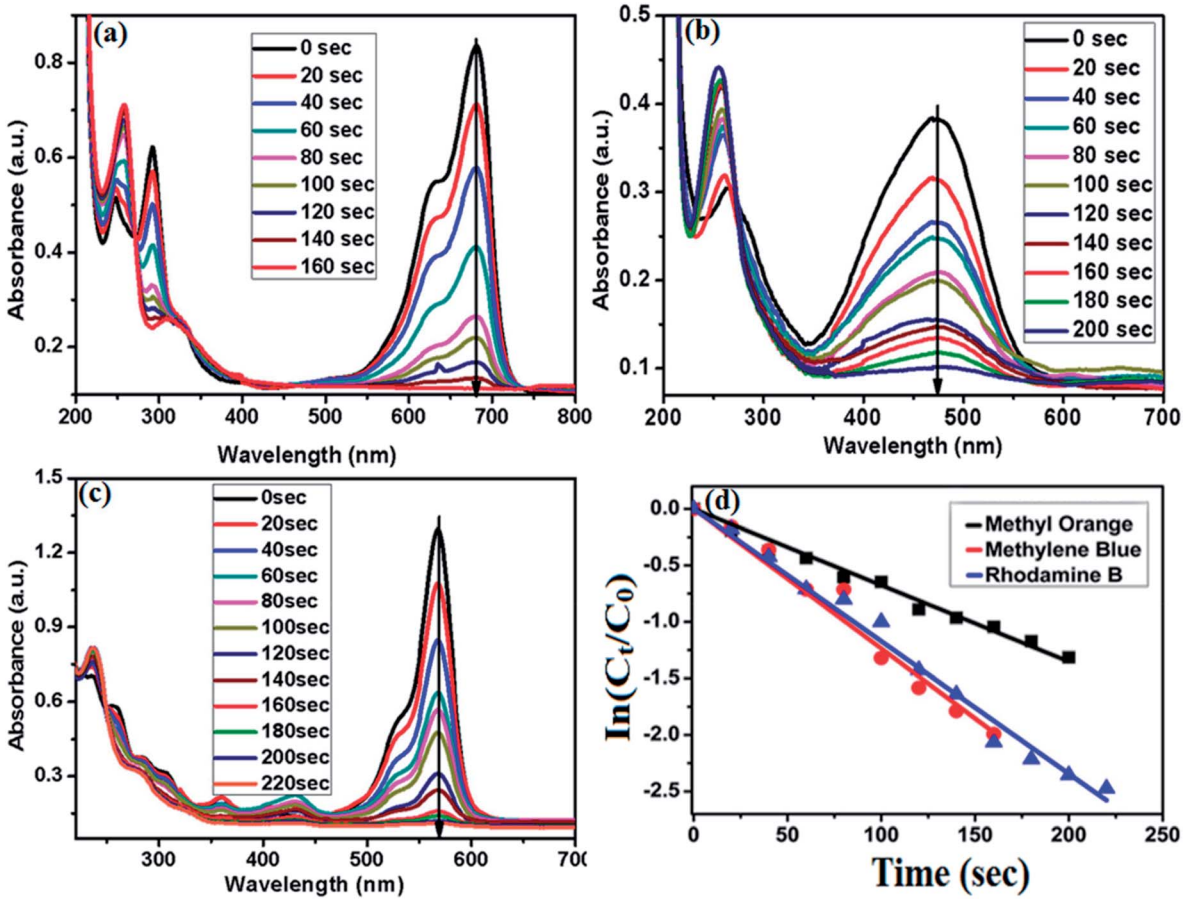

Fig. 10 UV-vis absorption spectra of degradation of 0.02 mM (a) RhB; (b) MO and (c) MB by $NaBH_4$ (0.1 M) in the presence of 0.2 mg of $cSiO_2$@DFNS@Ag as nanocatalyst and (d) plot of $\ln(C_t/C_0)$ *vs.* reaction time representing first order kinetics for the degradation of organic dyes.

Table 3 The correlation coefficient of $\ln(A_t/A_0)$ *vs.* time plot, reduction time, rate constant and activity parameter for the reduction of various organic dyes using $cSiO_2$@DFNS@Ag as nanocatalyst

Sample	R^2	Reduction time (s)	k ($NaBH_4$) ($\times 10^{-3}$ s^{-1})	Activity parameter ($K = s^{-1}$ g^{-1})
Methyl orange	0.995	200	6.76	33.8
Methylene blue	0.989	160	12.36	61.8
Rhodamine B	0.996	220	11.72	58.6

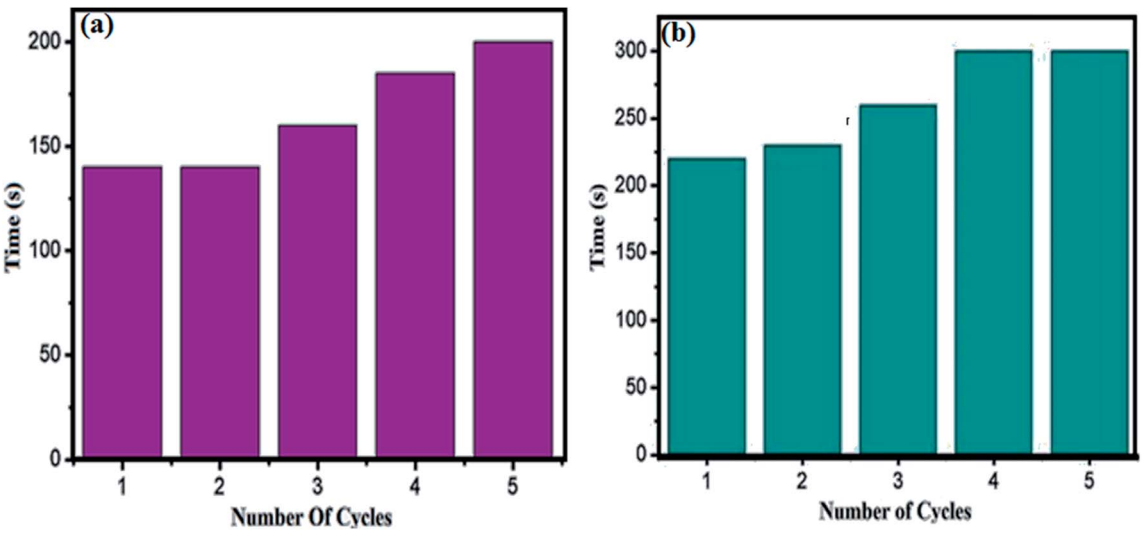

Fig. 11 Recyclability test of $cSiO_2$@DFNS@Ag nanocatalyst for (a) reduction of 4-NP and (b) degradation of RhB.

Following the completion of the reaction, the solid catalyst was separated from the reaction mixture and the reaction mixture was analysed by atomic absorption spectrophotometry (AAS) and leaching of silver nanoparticles in the reaction mixture was not detected through AAS. The accurate weight percentage of Ag in $cSiO_2$@DFNS@Ag after fifth catalytic cycle for the reduction of 4-NP was determined through ICP analysis and was found to be 2.98 wt%.

5. Conclusion

In conclusion, dendritic fibrous nanosilica over cubic core ($cSiO_2$@DFNS@Ag) was successfully developed using the surfactant-template approach. These particles were observed to have a uniform distance between the silica fibres from the outer surface to the interior core (nanoscopic space) due to cube like morphology. Subsequent to the characterization of the synthesized $cSiO_2$@DFNS by various available techniques, amine groups could be anchored on the fibres of $cSiO_2$@DFNS using APTES. Finally, silver nanoparticles could be immobilized on the amine functionalized $cSiO_2$@DFNS particles. These silver nanoparticles immobilized fibrous cubic silica particles ($cSiO_2$@DFNS@Ag) could be successfully employed as an efficient and recyclable catalyst for the reduction of toxic aromatic nitro compounds to their corresponding amines and degradation of organic dyes.

Conflicts of interest

There are no conflicts to declare.

References

1 V. Polshettiwar, D. Cha, X. Zhang and J. M. Basset, High-Surface-Area Silica Nanospheres (KCC-1) with a Fibrous Morphology, *Angew. Chem.*, 2010, **122**(50), 9846–9850.
2 Z.-M. Wang, W. Wang, N. Coombs, N. Soheilnia and G. A. Ozin, Graphene Oxide– Periodic Mesoporous Silica Sandwich Nanocomposites with Vertically Oriented Channels, *ACS Nano*, 2010, **4**(12), 7437–7450.
3 L. Xu, Y. Ren, H. Wu, Y. Liu, Z. Wang, Y. Zhang, J. Xu, H. Peng and P. Wu, Core/shell-structured TS-1@mesoporous silica-supported Au nanoparticles for selective epoxidation of propylene with H_2 and O_2, *J. Mater. Chem.*, 2011, **21**(29), 10852–10858.
4 D. Shen, J. Yang, X. Li, L. Zhou, R. Zhang, W. Li, L. Chen, R. Wang, F. Zhang and D. Zhao, Biphase stratification approach to three-dimensional dendritic biodegradable mesoporous silica nanospheres, *Nano Lett.*, 2014, **14**(2), 923–932.
5 Y.-J. Yu, J.-L. Xing, J.-L. Pang, S.-H. Jiang, K.-F. Lam, T.-Q. Yang, Q.-S. Xue, K. Zhang and P. Wu, Facile synthesis

of size controllable dendritic mesoporous silica nanoparticles, *ACS Appl. Mater. Interfaces*, 2014, **6**(24), 22655–22665.

6 Q. Yue, J. Li, W. Luo, Y. Zhang, A. A. Elzatahry, X. Wang, C. Wang, W. Li, X. Cheng and A. Alghamdi, An interface coassembly in biliquid phase: toward core–shell magnetic mesoporous silica microspheres with tunable pore size, *J. Am. Chem. Soc.*, 2015, **137**(41), 13282–13289.

7 X. Du, B. Shi, J. Liang, J. Bi, S. Dai and S. Z. Qiao, Developing Functionalized Dendrimer-Like Silica Nanoparticles with Hierarchical Pores as Advanced Delivery Nanocarriers, *Adv. Mater.*, 2013, **25**(41), 5981–5985.

8 X. Huang, Z. Tao, J. C. Praskavich Jr, A. Goswami, J. F. Al-Sharab, T. Minko, V. Polshettiwar and T. Asefa, Dendritic silica nanomaterials (KCC-1) with fibrous pore structure possess high DNA adsorption capacity and effectively deliver genes in vitro, *Langmuir*, 2014, **30**(36), 10886–10898.

9 Z. Sun, H. Li, D. Guo, J. Sun, G. Cui, Y. Liu, Y. Tian and S. Yan, A multifunctional magnetic core–shell fibrous silica sensing probe for highly sensitive detection and removal of Zn +2 from aqueous solution, *J. Mater. Chem. C*, 2015, **3**(18), 4713–4722.

10 M. Dhiman, B. Chalke and V. Polshettiwar, Organosilane oxidation with a half million turnover number using fibrous nanosilica supported ultrasmall nanoparticles and pseudo-single atoms of gold, *J. Mater. Chem. A*, 2017, **5**(5), 1935–1940.

11 A. Maity and V. Polshettiwar, Dendritic Fibrous Nanosilica (DFNS) for Catalysis, Energy Harvesting, CO_2 Mitigation, Drug Delivery and Sensing, *ChemSusChem*, 2017, **10**(20), 3866–3913.

12 R. Sharma, S. Sharma, S. Dutta, R. Zboril and M. B. Gawande, Silica-nanosphere-based organic–inorganic hybrid nanomaterials: synthesis, functionalization and applications in catalysis, *Green Chem.*, 2015, **17**(6), 3207–3230.

13 J. Wei, Z. Sun, W. Luo, Y. Li, A. A. Elzatahry, A. M. Al-Enizi, Y. Deng and D. Zhao, New Insight into the Synthesis of Large-Pore Ordered Mesoporous Materials, *J. Am. Chem. Soc.*, 2017, **139**(5), 1706–1713.

14 M. Bouhrara, C. Ranga, A. Fihri, R. R. Shaikh, P. Sarawade, A.-H. Emwas, M. N. Hedhili and V. Polshettiwar, Nitridated fibrous silica (KCC-1) as a sustainable solid base nanocatalyst, *ACS Sustainable Chem. Eng.*, 2013, **1**(9), 1192–1199.

15 Z. N. Siddiqui, K. Khan and N. Ahmed, Nano fibrous silica sulphuric acid as an efficient catalyst for the synthesis of β-enaminone, *Catal. Lett.*, 2014, **144**(4), 623–632.

16 S. M. Sadeghzadeh, A heteropolyacid-based ionic liquid immobilized onto fibrous nano-silica as an efficient catalyst for the synthesis of cyclic carbonate from carbon dioxide and epoxides, *Green Chem.*, 2015, **17**(5), 3059–3066.

17 L. Thankamony, A. Sofia, C. Lion, F. Pourpoint, B. Singh, A. J. Perez Linde, D. Carnevale, G. Bodenhausen, H. Vezin and O. Lafon, Insights into the Catalytic Activity of Nitridated Fibrous Silica (KCC-1) Nanocatalysts from 15N and 29Si NMR Spectroscopy Enhanced by Dynamic Nuclear Polarization, *Angew. Chem., Int. Ed.*, 2015, **54**(7), 2190–2193.

18 S. M. Sadeghzadeh, A heteropolyacid-based ionic liquid immobilized onto magnetic fibrous nano-silica as robust and recyclable heterogeneous catalysts for the synthesis of tetrahydrodipyrazolopyridines in water, *RSC Adv.*, 2016, **6**(79), 75973–75980.

19 A. Fihri, M. Bouhrara, U. Patil, D. Cha, Y. Saih and V. Polshettiwar, Fibrous nano-silica supported ruthenium (KCC-1/Ru): a sustainable catalyst for the hydrogenolysis of alkanes with good catalytic activity and lifetime, *ACS Catal.*, 2012, **2**(7), 1425–1431.

20 X. Le, Z. Dong, Y. Liu, Z. Jin, T.-D. Huy, M. Le and J. Ma, Palladium nanoparticles immobilized on core–shell magnetic fibers as a highly efficient and recyclable heterogeneous catalyst for the reduction of 4-nitrophenol and Suzuki coupling reactions, *J. Mater. Chem. A*, 2014, **2**(46), 19696–19706.

21 H. Yang, S. Li, X. Zhang, X. Wang and J. Ma, Imidazolium ionic liquid-modified fibrous silica microspheres loaded with gold nanoparticles and their enhanced catalytic activity and reusability for the reduction of 4-nitrophenol, *J. Mater. Chem. A*, 2014, **2**(30), 12060–12067.

22 M. Dhiman, B. Chalke and V. Polshettiwar, Efficient synthesis of monodisperse metal (Rh, Ru, Pd) nanoparticles supported on fibrous nanosilica (KCC-1) for catalysis, *ACS Sustainable Chem. Eng.*, 2015, **3**(12), 3224–3230.

23 Z. S. Qureshi, P. B. Sarawade, M. Albert, V. D'Elia, M. N. Hedhili, K. Köhler and J. M. Basset, Palladium Nanoparticles Supported on Fibrous-Structured Silica Nanospheres (KCC-1): An Efficient and Selective Catalyst for the Transfer Hydrogenation of Alkenes, *ChemCatChem*, 2015, **7**(4), 635–642.

24 K. Yu, X. Zhang, H. Tong, X. Yan and S. Liu, Synthesis of fibrous monodisperse core–shell Fe_3O_4/SiO_2/KCC-1, *Mater. Lett.*, 2013, **106**, 151–154.

25 D. Shen, L. Chen, J. Yang, R. Zhang, Y. Wei, X. Li, W. Li, Z. Sun, H. Zhu and A. M. Abdullah, Ultradispersed palladium nanoparticles in three-dimensional dendritic mesoporous silica nanospheres: toward active and stable heterogeneous catalysts, *ACS Appl. Mater. Interfaces*, 2015, **7**(31), 17450–17459.

26 N. Bayal, B. Singh, R. Singh and V. Polshettiwar, Size and Fiber Density Controlled Synthesis of Fibrous Nanosilica Spheres (KCC-1), *Sci. Rep.*, 2016, **6**, 24888.

27 J. S. Kang, J. Lim, W.-Y. Rho, J. Kim, D.-S. Moon, J. Jeong, D. Jung, J.-W. Choi, J.-K. Lee and Y.-E. Sung, Wrinkled silica/titania nanoparticles with tunable interwrinkle distances for efficient utilization of photons in dye-sensitized solar cells, *Sci. Rep.*, 2016, **6**, 30829.

28 X. Wang, Y. Zhang, W. Luo, A. A. Elzatahry, X. Cheng, A. Alghamdi, A. M. Abdullah, Y. Deng and D. Zhao, Synthesis of ordered mesoporous silica with tunable morphologies and pore sizes via a nonpolar solvent-assisted Stober method, *Chem. Mater.*, 2016, **28**(7), 2356–2362.

29 J. Shabir, C. Garkoti, D. Sah and S. Mozumdar, Development of Amine Functionalized Wrinkled Silica Nanospheres and Their Application as Efficient and Recyclable Solid Base Catalyst, *Catal. Lett.*, 2018, **148**(1), 194–204.

30 A. Kumar, S. Aerry, A. Saxena and S. Mozumdar, Copper nanoparticulates in Guar-gum: a recyclable catalytic system for the Huisgen [3 + 2]-cycloaddition of azides and alkynes without additives under ambient conditions, *Green Chem.*, 2012, **14**(5), 1298–1301.

31 A. Kumar, M. Dewan, A. De, A. Saxena, S. Aerry and S. Mozumdar, Aldol condensation in PEG-400 catalyzed by recyclable l-proline supported on nano gold surface, *RSC Adv.*, 2013, **3**(2), 603–607.

32 C. Garkoti, J. Shabir, P. Gupta, M. Sharma and S. Mozumdar, Heterogenization of amine-functionalized ionic liquids using graphene oxide as a support material: a highly efficient catalyst for the synthesis of 3-substituted indoles via Yonemitsu-type reaction, *New J. Chem.*, 2017, **41**(24), 15545–15554.

33 C. Garkoti, J. Shabir and S. Mozumdar, Imidazolium Based Ionic Liquid Supported on Fe_3O_4@SiO_2 Nanoparticle as an Efficient Heterogeneous Catalyst for N-formylation of Amines, *New J. Chem.*, 2017, **41**(17), 9291–9298.

34 J. Shabir, S. Rani, C. Garkoti and S. Mozumdar, Nitrolotriacetic acid assisted one step synthesis of highly stable silver nanoparticles in aqueous medium: investigation of catalytic activity, *Mater. Lett.*, 2017, **209**, 207–211.

35 J. Ge, Q. Zhang, T. Zhang and Y. Yin, Core–satellite nanocomposite catalysts protected by a porous silica shell: controllable reactivity, high stability, and magnetic recyclability, *Angew. Chem., Int. Ed.*, 2008, **47**(46), 8924–8928.

36 S. Tang, S. Vongehr and X. Meng, Carbon spheres with controllable silver nanoparticle doping, *J. Phys. Chem. C*, 2009, **114**(2), 977–982.

37 B. Naik, S. Hazra, V. S. Prasad and N. N. Ghosh, Synthesis of Ag nanoparticles within the pores of SBA-15: an efficient catalyst for reduction of 4-nitrophenol, *Catal. Commun.*, 2011, **12**(12), 1104–1108.

38 Z. Dong, X. Le, X. Li, W. Zhang, C. Dong and J. Ma, Silver nanoparticles immobilized on fibrous nano-silica as highly efficient and recyclable heterogeneous catalyst for reduction of 4-nitrophenol and 2-nitroaniline, *Appl. Catal., B*, 2014, **158**, 129–135.